Geomechanics and Engineering, *Vol. 34, No. 6 (2023) 637-648*
https://doi.org/10.12989/gae.2023.34.6.637

Shear behavior of foam-conditioned gravelly sands: Insights from pressurized vane shear tests

Shuying Wang[1,2,3], Jiazheng Zhong*[1,2], Qiujing Pan[1,2], Tongming Qu[4] and Fanlin Ling[1,2]

[1]*School of Civil Engineering, Central South University, Changsha, 410075, China*
[2]*Tunnel and Underground Engineering Research Center, Central South University, Changsha, 410075, China*
[3]*MOE Key Laboratory of Engineering Structure of Heavy Haul Railway, Central South University, Changsha, 410075, PR China*
[4]*Department of Civil & Environmental Engineering, The Hong Kong University of Science and Technology, Clearwater Bay, HKSAR, China*

(*Received September 9, 2022, Revised May 15, 2023, Accepted August 12, 2023*)

Abstract. When an earth pressure balance (EPB) shield machine bores a tunnel in gravelly sand stratum, the excavated natural soil is normally transformed using foam and water to reduce cutter wear and the risk of direct muck squeezing out of the screw conveyor (i.e., muck spewing). Understanding the undrained shear behavior of conditioned soils under pressure is a potential perspective for optimizing the earth pressure balance shield tunnelling strategies. Owing to the unconventional properties of conditioned soil, a pressurized vane shear apparatus was utilized to investigate the undrained shear behavior of foam-conditioned gravelly sands under normal pressure. The results showed that the shear stress-displacement curves exhibited strain-softening behavior only when the initial void ratio (e_0) of the foam-conditioned sand was less than the maximum void ratio (e_{max}) of the unconditioned sand. The peak and residual strength increased with an increase in normal pressure and a decrease in foam injection ratio. A unique relation between the void ratio and the shear strength in the residual stage was observed in the e-ln(τ) space. When e_0 was greater than e_{max}, the fluid-like specimens had quite low strengths. Besides, the stick-slip behavior, characterized by the variation coefficient of measured shear stress in the residual stage, was more evident under lower pressure but it appeared to be independent of the foam injection. A comparison between the results of pressurized vane shear tests and those of slump tests indicated that the slump test has its limitations to characterize the chamber muck fluidity and build the optimal conditioning parameters.

Keywords: foam mechanism; pressurized vane shear test; soil conditioning; stick-slip behaviour; undrained shear behaviour

1. Introduction

Earth pressure balance (EPB) shield machines use the excavated muck to balance the lateral earth pressure of strata at the excavation face during tunnelling. To create a condition suitable for tunnelling, some additives are normally used to condition the excavated muck into a paste with good workability, low shear strength, low adhesion strength, suitable compressibility, and low permeability during tunnelling (Thewes and Hollmann 2016, Huang *et al*. 2019, Wang *et al.* 2021, Bai *et al*. 2021). If the excavated soil is insufficiently conditioned, the high shear strength of muck may result in extra energy consumption and mechanical wear. On the contrary, if the excavated soil is excessively conditioned, the high permeability or fluidity can cause an uncontrolled outflow of the chamber muck and the loss of chamber pressure, eventually inducing tunnel face instability and excessive ground settlement (Peila 2014, Liu *et al.* 2020).

Many researchers adopted slump tests to assess the workability of the muck discharged from the screw conveyor, and hence give a fast evaluation of the conditioning effect when tunnelling in coarse-grained stratum (Quebaud *et al.* 1998, Budach and Thewes 2015, Wang *et al.* 2020). Table 1 shows the recommended ranges of slump values characterizing a desirable fluidity of conditioned coarse-grained soils in the existing literature. Different recommended ranges of slump values of coarse-grained soils were proposed in various projects, and there is no general standard for suitable conditioned coarse-grained soils. This indicates that the optimal soil conditioning scheme is influenced by the composition and gradation characteristics of soils. Moreover, the slump value is just an empirical characterization of the muck fluidity, which is associated with shear strength. The muck shear characteristics should be well comprehended because it not only determines the muck fluidity but also provides simulated parameters for a numerical model of muck transport in an EPB shield (Dang and Meschke 2020, Zhong *et al.* 2022). Numerical simulations of shield tunnelling could show the performance of tunnelling and discharging under different muck fluidities, shield geometries and tunnelling parameters.

Some laboratory methods have been adopted to evaluate the shear behavior of conditioned soil. The rotary shear test, initially designed to test the shear strength of clay (Zumsteg *et al.* 2012), is simpler to be performed and more suitable for soils with high fluidity. The specimen resembling a fluid is held in the container to its initial shape. Yang *et al.* (2020)

*Corresponding author, Ph.D. Student
E-mail: Jiazhengzhong@csu.edu.cn

http://www.techno-press.org/?journal=gae&subpage=7
ISSN: 2005-307X (Print), 2092-6219 (Online)

Table 1 Recommended slump range of coarse-grained soil

References	Soil types	Areas	Recommended slump range
Quebaud *et al*. (1998)	Siliceous sand	/	120 mm
Jancsecz *et al.* (1999)	Gravelly and silty sand	Izmir, Turkey	200~250 mm
Duarte (2007)	Leighton Buzzard sands and Thanet sand	/	100~150 mm
Peila *et al.* (2009)	Gravel and sand	/	150~200 mm
Budach and Thewes (2015)	Coarse-grained soil	/	100~200 mm
Martinelli *et al.* (2015)	Tar sand	/	150~200 mm
Ye *et al.* (2016)	Strongly weathered argillaceous siltstone	Nanchang, China	170~200 mm
Zhao *et al.* (2018)	Sandy pebble	Urumqi, China	205~210 mm
Wang *et al*. (2020)	Gravelly sand	Changsha, China	150~200 mm

investigated its rate-dependent shear behavior in large displacements based on rheology with the utility of a vane rheometer. Using a vane (Budach 2012), a sphere (Galli and Thewes 2019) or an auger (Hu and Rostami 2020; Hu and Rostami 2021) as a rotator, the shear strength of conditioned coarse-grained soil under atmospheric pressure was tested. The effect of conditioning parameters on rheological characteristics has been analyzed. The test specimens accord with the property proposed by Bezuijen (2012) that the porosity of conditioned soil should be larger than the maximum porosity. These conditioned soils behave as non-Newtonian fluids, meaning that the shear stress is invariable with shear displacements but associated with shear strain rates.

The shear behavior of the foam-conditioned soil under chamber pressures is expected to differ from that under atmospheric pressure due to the foam compressibility **(**Hu and Rostami 2020, Mori *et al.* 2018**)**. Martinelli *et al.* (2017) improved the conventional direct shear box and obtained the undrained strength of conditioned soils under different normal pressures. However, the stress distribution on the shear plane is nonuniform, resulting from the decreasing shear plane area during shearing. The triaxial test effectively determines the shear strength of coarse-grained soils at a three-dimensional stress state. To prepare and test a conditioned granular soil specimen behaving like a fluid in a large diameter triaxial cell, Martinelli *et al.* (2019) developed a new triaxial testing approach using an extension unloading stress path. This approach skips the vacuum-induced depression and mold removing to avoid foam bleeding and the specimen deformation before imposing confining pressures. Meng *et al.* (2011) designed a pressurized rheometer and found that different shear strengths of the conditioned coarse sand were displayed under different confining pressures. The vane had to overcome different shear strengths in different displacement stages, such as the peak and residual strength. Shear displacement, which is achieved in the pressurized vane shear test, can be high enough to enable the muck to reach the residual stage compared with the triaxial test. The peak strength can characterize the muck resistance to tool cutting, while the residual strength can reflect the muck resistance to flow in a pressurized chamber (Zhong *et al.* 2021). Therefore, fluid rheology is not suitable to explain the shear behavior of these conditioned sands. To date, little attention has been given to the shear behavior of pressurized foam-conditioned gravelly sands during a large shear displacement. Furthermore, the effect of conditioning agents on the vane shear strength under different pressures and its mechanism need to be further studied.

This paper aims to investigate the shear behavior of foam-conditioned gravelly sands during large shear displacements using a pressurized vane shear apparatus. Taking the maximum void ratio (e_{max}) of unconditioned sand as the threshold, the conditioned gravelly sands exhibit different types of shear stress-displacement relations. The influences of the normal pressure and conditioning parameters on the peak strength and residual strength are analyzed. The conditioning mechanism of foam on gravelly sand strength is revealed from a particle-scale perspective. The results of slump tests and vane shear tests are compared. Besides, the stick-slip behavior of conditioned gravelly sands in the residual stage is discussed in detail.

2. Material and approach

2.1 Testing material

The tested gravelly sand was collected from Jiujiang River in Jiangxi Province, China. Fig. 1 shows its grading curve. The coefficient of uniformity (C_u) and the coefficient of curvature (C_c) are 10.0 and 0.7, respectively. The testing gravelly sand is classified as poorly graded gravelly sand according to GB/T50145 (Standardization Administration of the People's Republic of China, 2007), while it is classified as poorly graded sand with gravel according to ASTM D2488-17 (American Society for Testing and Material, 2017). Additionally, the particle density (ρ_s) is 2.65 g/cm^3, and e_{max} is 0.768.

The soil specimen was conditioned by water and foam, which are commonly adopted in EPB shield tunnelling. The representative parameters that denote the foam properties are the concentration of the foaming agent solution (C_f), the foam expansion ratio (FER), and the half-life period ($t_{50\%}$). The parameters are defined as follows:

C_f indicates the concentration of the foaming agent in its foaming agent solution, as expressed in Eq. (1).

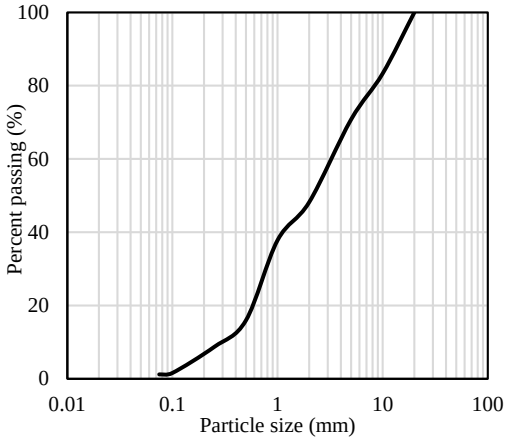

Fig. 1 Grain size distribution for the soil specimen

$$C_f = \frac{V_{fa}}{V_{fas}} = \frac{V_{fa}}{V_{fa}+V_w} \times 100\% \quad (1)$$

where V_{fas} is the volume of the foaming agent solution; V_{fa} is the volume of the foaming agent; V_w is the volume of water required for dilution.

FER, reflecting the dilatancy of the foaming agent solution, can be defined as Eq. (2)

$$FER = \frac{V_f}{V_{fas}} \quad (2)$$

where V_f is the volume of injected foam.

$t_{50\%}$, reflecting the stability of foam, indicates the required time for the degradation of 50% of foam.

The C_f of the selected foaming agent solution was determined to be 3%; the *FER* of the foaming agent was10.0; the $t_{50\%}$ of the foam was 7.5 min. The above foam properties meet the demand that C_f should be in the range of 0.5~5%, *FER* be in the range of 5~30 and $t_{50\%}$ be longer than 5 min for EPB shield tunnelling (EFNARC 2005).

As the key parameters affecting the shear characteristics of the muck in an EPB shield machine, the water content (*w)* and the foam injection ratio (*FIR)* were changed to study their conditioning effects on gravelly sands. *FIR* is defined as follow

$$FIR = \frac{V_f}{V_s} \times 100\% \quad (3)$$

where *Vs* is the volume of the unconditioned soil.

Table 2 provides the conditioning parameters of soil specimens and the corresponding slump values. Furthermore, Fig. 2 shows the variation of the slump values under different conditioning cases. Specimens No. 1~5 were set as the experimental group with different *FIR*s to investigate the conditioning effect of foam on shear characteristics under different pressures. The slump value initially decreased and then increased with increasing FIR, which was consistent with the observation in Wang et al (2020). Additionally, Specimens No. 3, 6, 7, and 8 with similar slump values but various conditioning parameters were set as the other group to investigate the conditioning

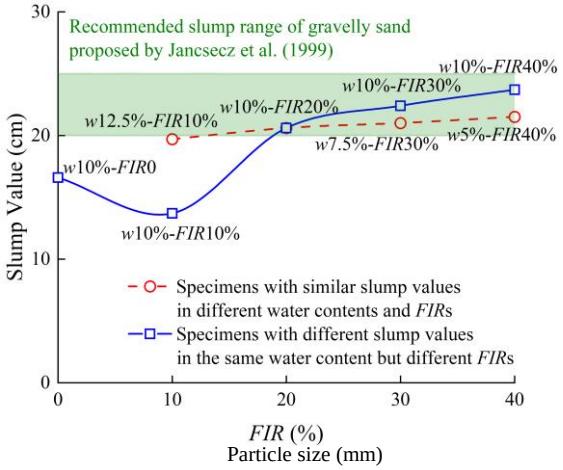

Fig. 2 Comparison of slump values for different conditioned gravelly sands

Table 2 Conditioning parameters and fluidity indexes of different specimens under atmospheric pressure

Specimen No.	Conditioning parameters		Slump Value (mm)
	Water content *w* (%)	Foam injection ratio *FIR* (%)	
1	10	0	166
2	10	10	137
3	10	20	206
4	10	30	224
5	10	40	232
6	5	40	220
7	7.5	30	210
8	12.5	10	196

effects of water and foam and the applicability of slump values to evaluate the soil shear behavior under different pressures.

2.2 Testing apparatus

The suitable conditioned soils have relatively low permeability and can be efficiently transported out of the chamber and the screw conveyor during tunnelling (Wang *et al.* 2021). Therefore, the flowing muck barely drains. The pressurized rotary shear apparatus (Liu *et al.* 2019) was used to study the undrained shear behavior of conditioned gravelly sands. As shown in Fig. 3, the apparatus mainly consists of a container, a driver for applying the normal pressure, a driver for rotating the vane, some monitoring elements, and a data acquisition system. The container has an internal diameter (*D*) of 200 mm and a height (*H*) of 200 mm. The normal pressure uniformly transmitted to the specimen through the beam and top plate simulates the pressurized environment so that the shear behavior of specimens is studied under real stress states in the pressurized chamber of an EPB shield machine. The vane is driven by a motor and a reduction gear at any constant rotation rate from 0 to 60 rpm to achieve different strain rates under shearing conditions.

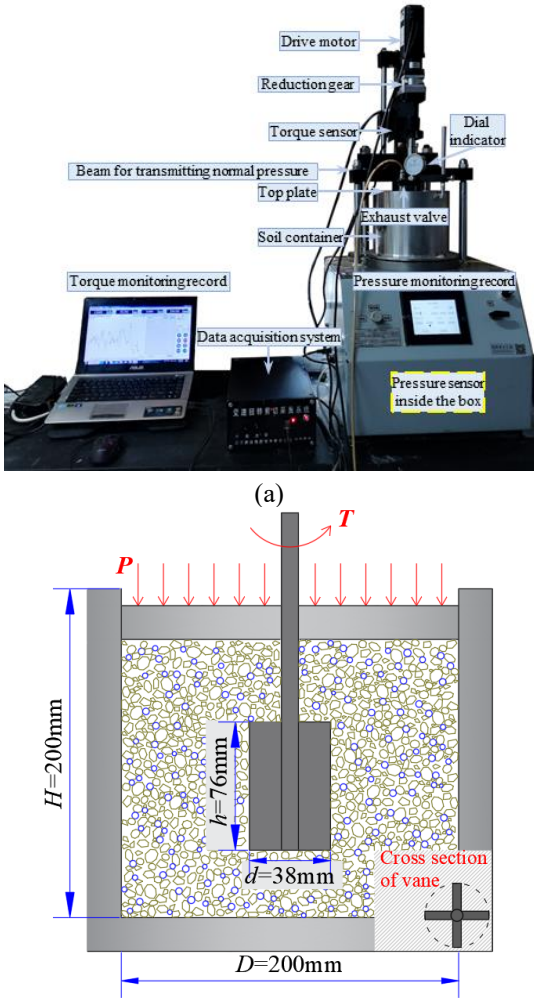

Fig. 3 Pressurized vane shear apparatus: (a) photo of the apparatus and (b) schematic diagram

It is recommended in ASTM D4648-2011 (American Society for Testing and Material, 2011) that the clearance between the shear interface and the outer edge of the specimen is at least two times the vane diameter, and the vane height is twice larger than the vane diameter. The diameter (d) and height (h) of the used vane are 38 mm and 76 mm, respectively. Therefore, the clearance in the container is 81 mm, which is more than two times its vane diameter (38 mm). The ratio of height to diameter also follows the recommendation. The monitoring elements include a dial indicator, a pressure sensor, and a torque sensor. The dial indicator records the vertical deformation of the specimen during normal compression and vane shearing. The pressure sensor shows the applied normal pressure in the capacity range of 0~200 kPa. The torque sensor monitors the torque of the vane in the capacity range of 0~30 N·m. The normal pressure (p) and vane torque (T) can be recorded by the data acquisition system. It might be an alternative perspective to monitor excess pore pressures near the rotating vane to understand its effect on muck shear characteristics. However, pore pressure sensors cannot be installed near the vane in the current shape, resulting in the response of excess pore pressure to the vane shearing being unknown in this study.

In addition, Zhang (2014) recommended that the clearance in the container should be three times larger than the largest grain diameter. In the current study, the tested soil had largest grain diameter of 19 mm, and so the clearance (81 mm) in the container was at least 4.3 times larger than the largest grain diameter of the tested soil.

2.3 Testing procedures and conditions

Each vane shear test was carried out step-by-step as follows:

1) The dry gravelly sand, water, and foam were well mixed in a mixer for 60 s, and then the mixture was evenly placed in the container layer by layer. Each specimen was prepared in three layers, each of which has a thickness of about 6 cm. The weight of soil for each layer was controlled to be identical.

2) Through the central hole in the top plate, the vane was put into the center of the specimen (see Fig. 3(b)). Afterward, the top plate was positioned. With the exhaust valve at the top plate open, a normal pressure of 10 kPa was applied to expel the air at the specimen's top surface.

3) The exhaust valve was closed for supplying an undrained condition for an experimental test. Then, the desired pressure was applied to the specimen through the top plate. The undrained specimen was compressed mainly due to the pressure-induced contraction of foam bubbles. When the dial indicator reading was constant, the volumetric deformation of the specimen due to normal compression was recorded. The void ratio after compression was calculated for each test. Table 3 shows the initial void ratios (e_0) of different specimens

4) Referring to the standard of the vane shear test method in GB/T50123-2019 (Standardization Administration of the People's Republic of China, 2019), the vane was rotated at a constant rate of 1/30 rpm. The vane torque was monitored and recorded every 0.1 degrees to determine the shear strength of each specimen.

5) The recorded whole torque consists of the shaft torque due to the friction at the inner wall of the central hole in the top plate and the vane torque due to the shear resistance of the soil specimen. The shaft torque can be obtained when rotating the vane in the absence of soil in the container. Therefore, the actual vane torque related to the shear stress of specimens is determined by subtracting the shaft torque from the whole torque.

6) The measured vane torque fluctuated during shearing due to the inhomogeneous distribution of particles in different sizes. The dial indicator reading and the vane torque would tend to be low and constant, i.e., the volume and the shear stress of the specimen were invariant with increasing shear strain in the residual stage, meaning that the shearing specimen had reached its ultimate state. Therefore, to obtain a sufficiently large shear displacement of the specimen to capture the residual torque and void ratio in the residual stage, the vane was driven to a rotation angle as large as 1440° (4 cycles) in tests.

Given that the saturation S_r of compressed specimens

Table 3 Initial void ratios of the specimens under different testing cases

No.	w (%)	FIR (%)	Normal pressure (kPa)				
			0	50	100	150	200
1	10	0	0.763	0.724	0.685	0.659	0.657
2	10	10	**0.813**	0.729	0.708	0.671	0.668
3	10	20	**0.877**	0.755	0.713	0.679	0.675
4	10	30	**0.948**	**0.770**	0.727	0.690	0.678
5	10	40	**1.071**	**0.809**	0.752	0.698	0.685
6	5	40	**0.963**	**0.795**	0.718	0.688	0.683
7	7.5	30	**0.935**	0.763	0.714	0.685	0.677
8	12.5	10	**0.838**	0.744	0.713	0.678	0.670

*Note: The data in bold represent the cases in which e_0 is larger than the e_{max} (0.768) of the unconditioned gravelly sand

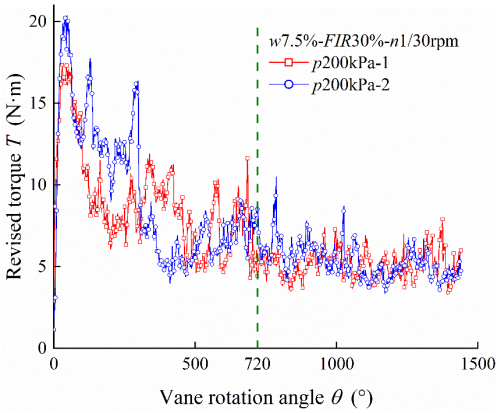

Fig. 4 The repeated results of vane shear tests under the same condition

under variable pressure range from 0.3 to 0.5, calculated as Eq. (4). The tested soil specimens are unsaturated.

$$S_r = \frac{wG_s}{e_0} \tag{4}$$

where G_s is the specific gravity of a specimen.

The test scheme was repeated to verify its reliability. As shown in Fig. 4, only a small difference in the measured torque-rotation angle curves was observed between the two tests with the same testing conditions, indicating that the proposed test scheme was reliable for investigating the shear behavior of conditioned gravelly sands.

Urban tunnels are usually buried 10 ~ 30 m in depth in China, so the maximum chamber pressure in an EPB shield is commonly controlled within 200 kPa (Zhang 2009). Therefore, this study set the normal pressures applied to the specimens to 0, 50, 100, 150, and 200 kPa, respectively.

3. Testing results

3.1 Shear stress-displacement relation

In the shearing process, the shear failure interface, on which the relative shear displacement occurred, is generated by the rotating vane. The size of the cylindrical failure interface depended on the vane diameter (d) and height (h).

The relation between the shear displacement (u) and vane rotation angle (θ) is given in Eq. (5). According to ASTM D4648-2011 (American Society for Testing and Material, 2011), it is assumed that the shear stress on the failure interface is identical and evenly distributed, so the undrained shear stress (τ) can be calculated from the recorded vane torque (T), as shown in Eq. (6).

$$u = \frac{\pi\theta d}{360} \tag{5}$$

$$\tau = \frac{6T}{\pi\left(d^3 + 3d^2h\right)} \tag{6}$$

Depending on the initial void ratio of foam-conditioned specimens, two different evolution patterns (Type I and Type II) of shear stress–displacement relation, i.e., the τ-u relation were observed (see Fig. 5). The e_{max} could be regarded as the threshold.

Type I: Take specimens with 'w10%-FIR20%' under different normal pressures ranging from 50 kPa to 200 kPa as examples, Fig. 5 (a) shows the typical τ-u curves when e_0 is smaller than e_{max}. The shear stress initially grew as the shear displacement increased. The shear stress reached its peak value until the shear failure interface was formed, changing from 10.0 kPa to 80.0 kPa for the four cases. Then, the shear stress gradually decreased with an increase in the shear displacement. Afterwards, the shear stress tended to fluctuate within a certain range with the increasing shear displacement, where the reconstituted specimen continued to distort without significant changes in the shear stress. Moreover, the shear stress in the whole shear process increased accordingly with an increase in normal pressure.

Due to the shear stress fluctuations, strength characteristics are hardly obtained from measured shear stress-displacement curves. To eliminate the interference of stress fluctuations on determining the shear characteristic parameters, the measured τ-u curves need to be fitted. Eqs. (7)-(9) proposed by Cao *et al.* (2012) were successfully used to fit the τ-u curves with strain-softening characteristics.

$$\tau = \begin{cases} k_s u & (\tau \le \tau_s) \\ \left(k_s u - \tau_r\right)\exp\left[-\left(\frac{\tau - \tau_s}{n}\right)^m\right] + \tau_r & (\tau > \tau_s) \end{cases} \tag{7}$$

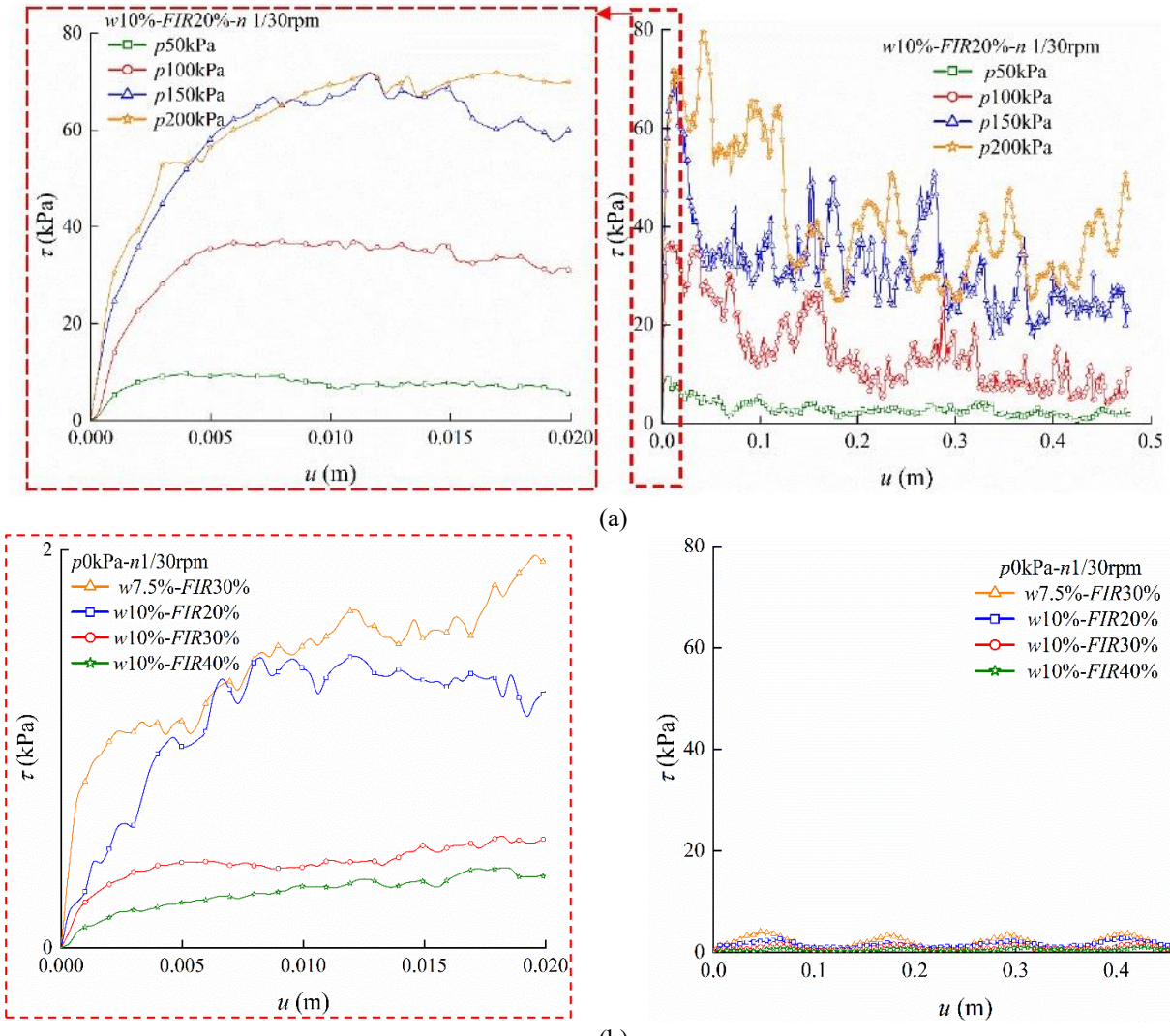

Fig. 5 Typical shear stress-displacement curves of the specimens: (a) Type I: curves with the strain-softening characteristics and (b) Type II: curves without the strain-softening characteristics (taking some testing cases as examples)

$$m = \frac{k_s u_f - \tau_s}{\left(k_s u_f - \tau_r\right) \ln \dfrac{k_s u_f - \tau_r}{\tau_f - \tau_r}} \tag{8}$$

$$n = \left(k_s u_f - \tau_s\right) \left[\ln \frac{k_s u_f - \tau_r}{\tau_f - \tau_r} \right]^{-\frac{1}{m}} \tag{9}$$

where τ_s is the yield strength; k_s is the shear stiffness at the elastic stage; τ_r is the residual strength; m and n are are described as Eqs. (8) and (9); τ_f is the peak strength; u_f is the required shear displacement for reaching the peak strength.

Taking the specimen with 'w10%-*FIR*20%' as an example, Fig. 6 shows the best-fitted τ-u curves with strain-softening characteristics under different normal pressures. The nominal values of the initial shear stiffness, yield strength, peak strength, and residual strength are easily determined.

Type II: Take four specimens with different conditioning parameters under atmospheric pressure as examples, Fig. 5 (b) shows the typical τ-u curve when e_0 is greater than e_{max}.

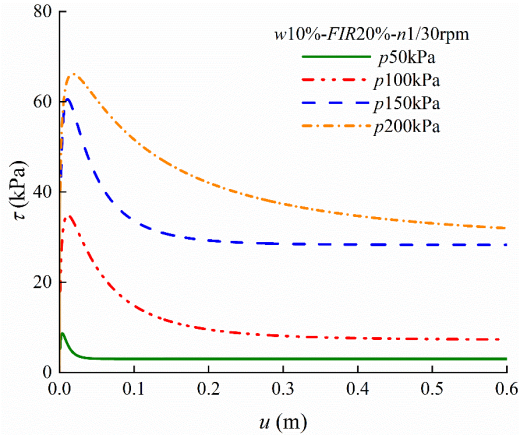

Fig. 6 Best fitting Type I shear stress-displacement curves of the Specimen 'w10%-*FIR*20%

The shear stress had a little increase as the vane began to

rotate and then tended to fluctuate regularly with a constant peak as the shear displacement increased. The measured shear stress was between 1.0 kPa to 4.0 kPa for the four specimens, which is much less than the shear stress of specimens with its e_0 smaller than e_{max}. Unlike the specimen of Type I with a peak strength, the specimen of Type II showed no strain-softening characteristics during shearing.

The specimens behaved like a fluid with suspending particles because foam bubbles uplifted sand particles and the particle system of the specimen had almost no effective stress (Bezuijen 2012). After eliminating the initial stage of τ-u curves with an increase in τ from zero, the average value of measured shear stress of the fluid-like specimen was taken as the nominal residual strength.

3.2 Shear stress fluctuations

As shown in Fig. 5, the τ-u curve of conditioned gravelly sand was accompanied by obvious stress fluctuations, particularly in the residual stage. The irregular shear stress fluctuations in Type I curves can be attributed to the stick-slip behavior (Albert 2000). Granular materials like gravelly sands transmit forces via interparticle contacts, and inhomogeneous force networks tend to be developed inside the materials to balance external loads (Qu *et al.* 2021). These force networks evolve gradually during shearing due to continuous break and reconstruction of force chains. When strong force chains break, a sudden reduction in the shear stress may be observed during shearing. As the shear deformation continues, new strong force chains develop and then the measured stress comes back immediately (Qu *et al.* 2019). Such a stick-slip behavior is more evident for the coarse-grain soil in contrast to clay or fine sands (Adjemian and Evesque 2004). The latter normally shows smooth shear stress-strain curves during vane shearing (Meng *et al.* 2011).

When e_0 is greater than e_{max}, foam bubbles, as easily compressible mediums, almost uplift sand particles. As a result, contact forces cannot be transmitted between sand particles, and so the stress fluctuations are inapparent.

3.3 Effect of normal pressure and FIR on shear strength

Fig. 7 shows the variations of the initial void ratio and the peak strength against the normal pressures for the specimens with different *FIR*s. The specimens whose e_0 were greater than e_{max} had no peak strength so they are out of the scope of this discussion. As the normal pressure increased, the initial void ratio decreased due to the compression of foam bubbles and the peak strength increased. Fig. 7 also showed that *FIR* was positively correlated with the initial void ratio. The increasing *FIR* significantly reduced the peak strength. The measured effect of normal pressure and *FIR* on conditioned soil strength agrees with the observations made in the existing literature (Mori et al. 2018, Galli and Thewes 2019).

Fig. 8 shows the variations of the residual strength and the corresponding void ratio against the normal pressure for the specimens with different *FIR*s. When e_r was greater than

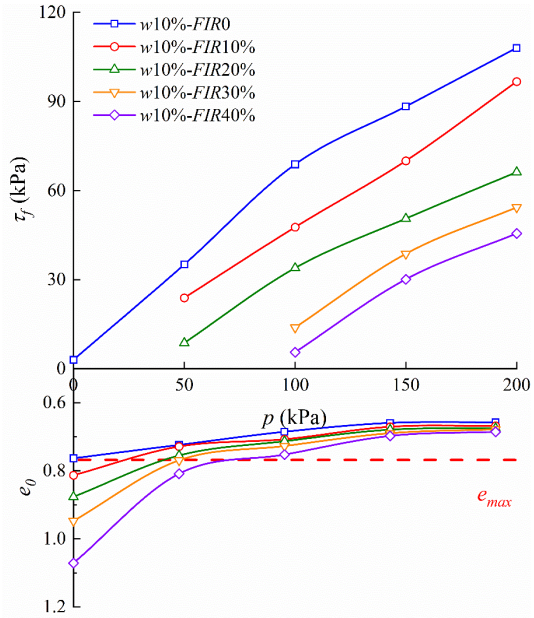

Fig. 7 Variation of the initial void ratio and peak strength against normal pressure for the specimens with different FIRs

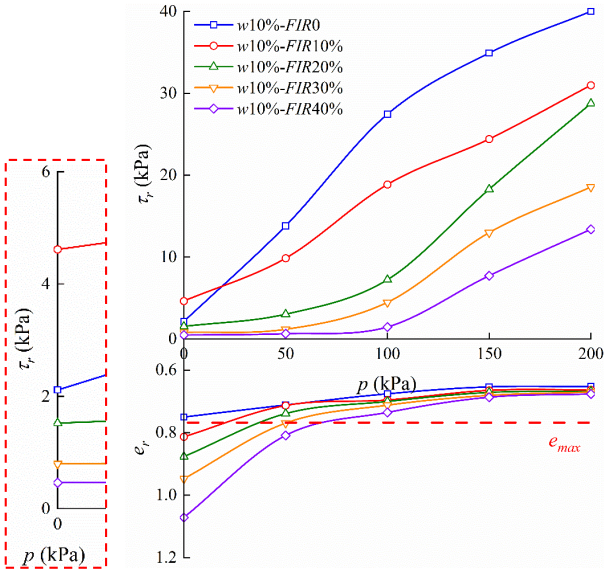

Fig. 8 Variation of the void ratio and shear strength in the residual stage against normal pressure for the specimens with different *FIR*s

e_{max}, the residual strength was quite low no matter how much normal pressure was applied. When e_r was smaller than e_{max}, the void ratio in the residual stage decreased and the residual strength increased with an increase in normal pressure.

As shown in the zoomed image on the left side of Fig. 8, the residual strength under atmospheric pressure (p = 0) increased from 3.0 kPa at *FIR* = 0 to 4.5 kPa at *FIR* = 10%, beyond which it decreased with an increase in *FIR*. The specimen with *FIR* = 10% had the highest strength under p = 0, explaining why it had the minimum slump value as observed in Fig. 2. The slump value offered a good

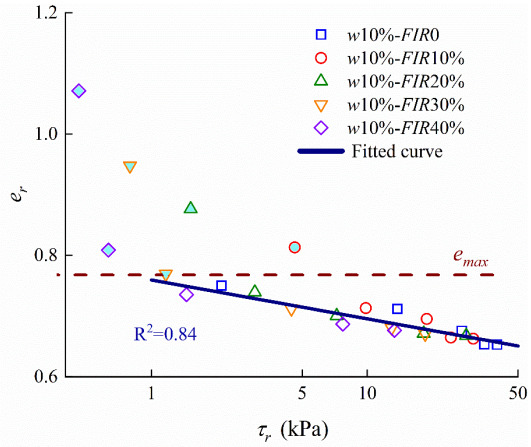

Fig. 9 Variation of the residual strength against the corresponding void ratio for the specimens with different *FIR*s

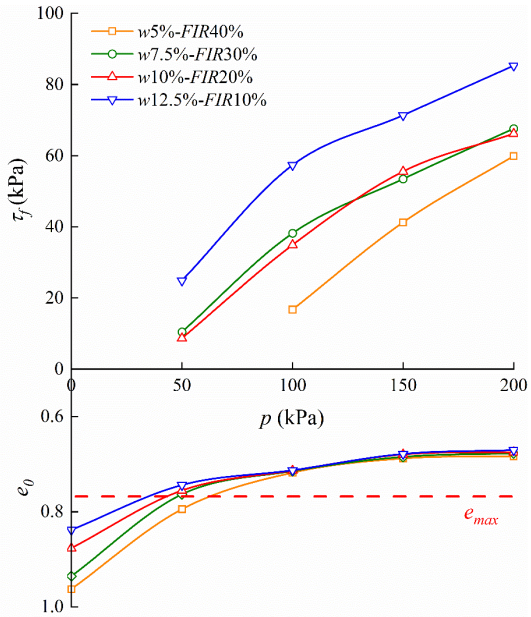

Fig. 10 Variation of the initial void ratio and peak strength against normal pressure for the specimens with similar slump values

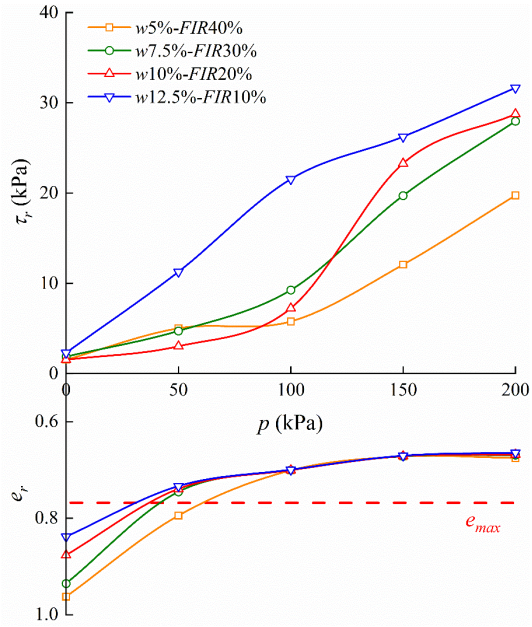

Fig. 11 Variation of the void ratio and shear strength in the residual stage against normal pressure for the specimens with similar slump values

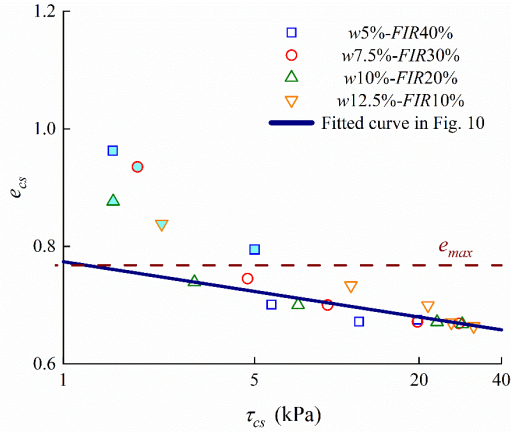

Fig. 12 Variation of the residual strength against the corresponding void ratio for the specimens with similar slump values

correlation with the residual strength under $p = 0$. However, the residual strength reduced with an increase in *FIR* under $p > 0$.

Fig. 9 shows that the void ratio and shear strength in the residual stage of the specimens with different *FIR*s follow the same unique relation in the e-ln(τ) space when e_r is smaller than e_{max}. It proved that the residual strength of conditioned gravelly sands was negatively correlated to the void ratio in the residual stage. However, when e_r is greater than e_{max}, the e_r-ln(τ_r) relation of fluid-like conditioned gravelly sands disobeyed the unique line.

3.4 Comparison of the effect of water and foam on shear strength

Fig. 10 shows the initial void ratio and the peak strength of the four specimens with similar slump values (see Fig. 2) under different normal pressures. Similar to the results in Fig. 7, the peak strength generally increased with the normal pressure for each conditioning case. When e_0 was smaller than e_{max}, the specimen with '*w*12.5%-*FIR*10%' had the lowest initial void ratio but the highest peak strength, while the specimen with '*w*5%-*FIR*40%' had the largest initial void ratio but the lowest peak strength. The specimens with the conditioning parameters '*w*10%-*FIR*20%' and '*w*7.5%-*FIR*30%' had a similar effect on the peak strength.

Fig. 11 shows the void ratio and the shear strength in the residual stage for the specimens with similar slump values under different normal pressures. The residual strengths of these specimens were almost the same under $p = 0$, explaining why these specimens had nearly the same slump values (see Fig. 2). Similar to the results in Fig. 8, the residual strength grew and the corresponding void ratio

reduced with an increase of the normal pressure. Moreover, the specimen conditioned with higher *FIR* and lower water content had lower residual strength. As shown in Fig. 12, when e_r was smaller than e_{max}, the e_r-ln(τ_r) relation still followed the unique relation in Fig. 9

The results show that Δw = 2.5% and ΔFIR = 10% have the same effect on conditioned soil strength under p = 0, but the latter is more effective for weakening the strength under p > 0. In other words, the slump test results hardly reflect the difference in conditioned soil strength between the sand specimens with various conditioning parameters under p > 0.

4. Discussion

4.1 Stick-slip behavior of conditioned gravelly sands in the residual stage

As presented previously, the shear deformation of conditioned gravelly sands with e_r smaller than e_{max} in the residual stage was accompanied by the stick-slip behavior of shear stress (see Fig. 5). Otherwise, the conditioned gravelly sands with e_r greater than e_{max} showed little stick-slip behavior. Furthermore, the repeated damage and reconnection of the strong force chains of the particle system possibly causes the extra unexpected pressure fluctuation in the chamber, potentially having some negative influences on the excavation face instability. Therefore, it is necessary to analyze the degree of the stick-slip behavior of shear stress under different testing cases. The coefficient of variation is introduced to characterize the degree of stick-slip behavior after the specimens reach the residual stage. The greater the coefficient of variation is, the more obvious the stick-slip behavior is. The shear displacement used for calculating the coefficient of variation in the residual stage is in the range of 0.24 ~ 0.48 m, corresponding to the vane rotation angle varying among 720°~1440° mentioned in Section 2.3. The coefficient of variation (c_v) is calculated as follow

$$c_v = \frac{\sqrt{\frac{\sum_{i=1}^{n}(\tau_i - \tau_r)^2}{n}}}{\tau_r} \tag{10}$$

where τ_i is the measured shear stress of the specimens in the residual stage.

Fig. 15 shows the coefficient of variation of shear stress in the residual stage for different specimens. Fig. 15(a) shows that as the applied normal pressures increased in the range of 0~200 kPa, the coefficient of variation firstly decreased and tended towards constant. Therefore, the results reveal that the stick-slip behavior of flowing muck at the top of the pressurized chamber and near the outlet of the screw conveyor needs more concerns. Fig. 15(b) shows that the coefficient of variation changed slightly with an increase in *FIR*, so that the degree of stick-slip behavior in the specimens with different *FIR*s had almost no difference.

4.2 Conditioning mechanism of foam under pressure

To promote the understanding on the effect on the shear behavior of pressurized conditioned gravelly sand, a particle-scale mechanism shown in Fig. 13 is introduced here. The particle-scale origins of the macroscopic shearing resistance in granular soils involve the interparticle interlocking and the sliding friction (see Fig. 13(a)). The former origin determines that the shear strength of granular soils is pressure-dependent or effective stress-dependent in the presence of water. The relative particle slip should overcome the sliding frictional strength associated with surface microroughness. The geometrical interlocking restricts the climbing of particles over adjacent ones and the dilation of the granular mass (Terzaghi *et al.* 1996). The peak strength depends on the sliding friction and the geometrical interlocking. However, the rearranged particles are orientated parallel to the failure interface during shearing in the residual stage. The residual strength is mainly determined by the sliding friction.

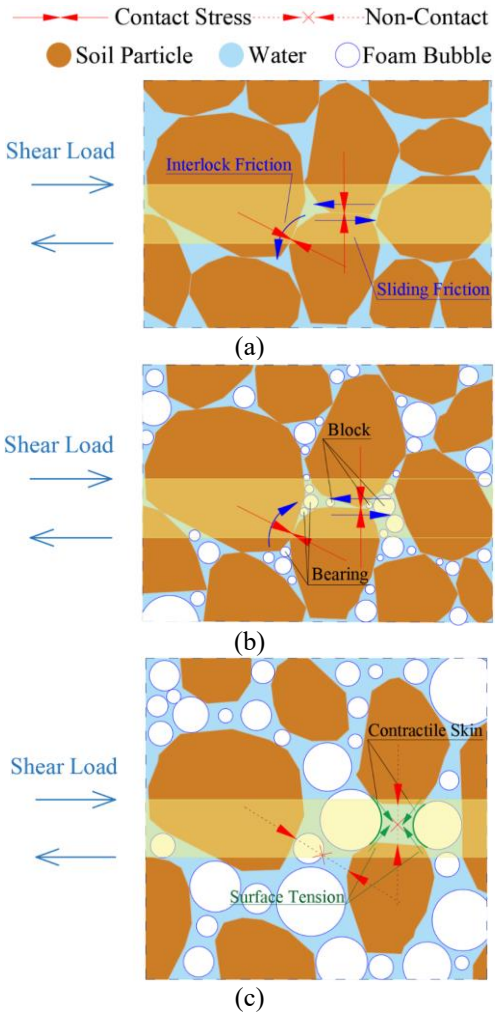

Fig. 13 Schematic of shearing resistance and foam effect in pressurized conditioned gravelly sand during shearing: (a) Specimens without foam, (b) Specimens with foam when e_0 is smaller than e_{max} and (c) Specimens with foam when e_0 is greater than e_{max}

As for specimens with e_r smaller than e_{max}, the void ratio reduced with an increase of normal pressure, meaning that the sand skeleton and internal bubbles contracted. The increasing contact area between particles created more

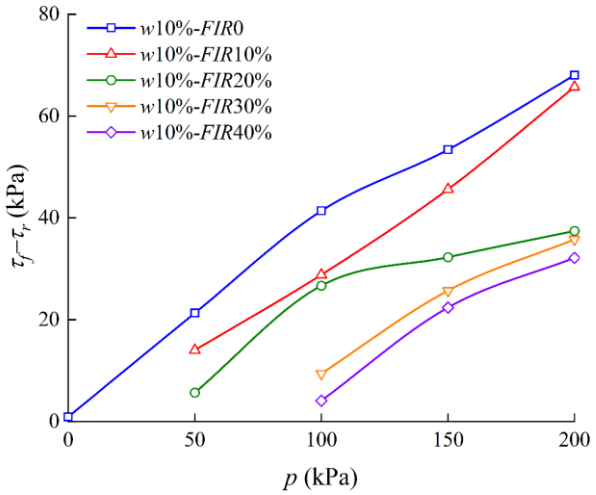

Fig. 14 Variation of the strength difference against normal pressure for the specimens with different *FIR*s

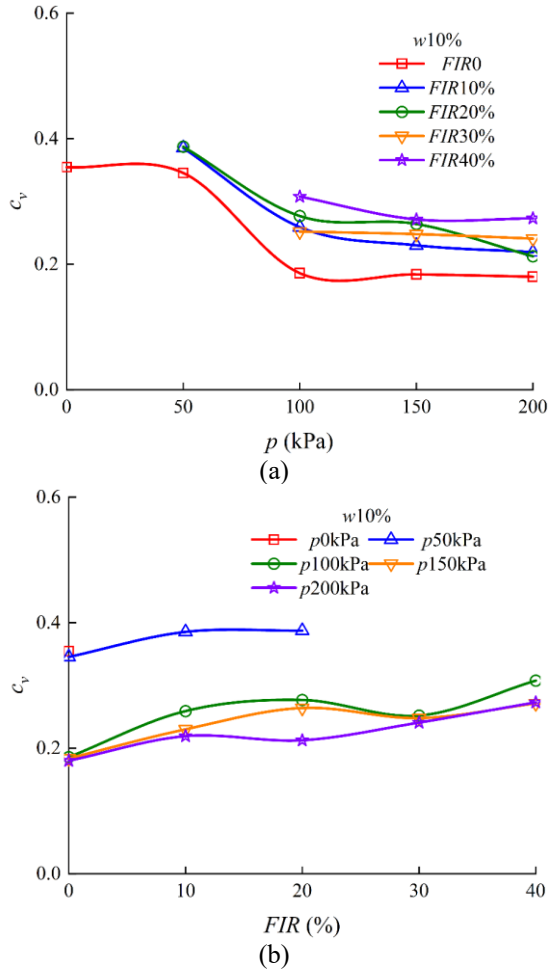

Fig. 15 Coefficient of variation of shear stress in the residual stage with varying: (a) Normal pressure and (b) *FIR*

stress transmission paths in the skeleton, leading to greater sliding friction needed to overcome during shearing and greater residual strength (see Fig. 8).

In terms of the effect of FIR on the shear strength of gravelly sand, there are two possible reasons why the sliding friction decreases with an increase of *FIR*. On the one hand, the increasing *FIR* makes more bubbles fill in pores and expands the void ratio. More stress originally supported by the sand skeleton is transferred to pore pressure by foam bubbles, which are in contact with sand particles, resulting in less sliding friction (see Fig. 13(b)). On the other hand, the lubrication of the foam solution on particle surfaces contributed to the decrease of the sliding friction coefficient (Vinai *et al.* 2008). However, the unique e_r-ln(τ_r) relation of the conditioned gravelly sands when e_r was smaller than e_{max} proved that the main effect of foam bubbles on decreasing the sliding friction is expanding the void ratio and transferring some skeleton stress to pore pressure.

Furthermore, the difference between peak strength and residual strength can reflect the contribution of the geometrical interlocking friction to the peak strength. Fig. 11 shows that the strength difference increased with the normal pressure and decreased with *FIR*. The increasing normal pressure makes particles denser and increases the distance of particles climbing and the interparticle contact force, resulting in greater geometrical interlocking friction.

The foam bubbles play a role of ball bearing, so the particles are looser to restrain the dilatancy and the foam bubbles make particle climbing easier as an increase of *FIR* (see Fig. 10(b)). The energy required for the climbing of particles over adjacent particles is decreased with increasing *FIR*.

In addition, the interparticle contact of specimens with e_r greater than e_{max} is blocked by foam bubbles. However, the surface tension at the contractile skin of bubbles pulls adjoining particles together (see Fig. 13(c)). The stress-independent strength attributed to the surface tension has the same effect as if the granular materials have a certain amount of cohesion, known as apparent cohesion (Xu and Du 2019).

4.3 Engineering inspirations based on test results

The results of different peak and residual strengths of pressurized conditioned gravelly sands demonstrate that the foam injection can facilitate cutting soil during excavation and promote muck fluidity during discharging. However, the soil conditioning effect of foam would be weakened with an increase in ambient pressure. It should be mentioned that the slump value determined by the apparent cohesion-related strength of the discharged muck may mislead the assessment of the stress-dependent strength in a pressurized chamber.

In addition, a series of slump tests of soils with different conditioning parameters are commonly used to determine some conditioning schemes that achieve the suitable conditioning state of muck for EPB shield tunnelling (Ye *et al.* 2016, Wang *et al.* 2020). However, the conditioned gravelly sands with similar slump values but different water contents and *FIR*s showed various strength characteristics under different ambient pressures. Therefore, this method with the slump tests may be insufficient to obtain the suitable fluidity of muck in a chamber and guide smooth tunnelling.

5. Conclusions

A pressurized vane shear apparatus was used to investigate the shear characteristics of foam-conditioned gravelly sands in the peak and residual stages. The effect and mechanism of foam and water on the shear strength under ambient pressure were discussed. The conclusions are obtained as follows:

- The shear behavior of foam-conditioned sand depends on the initial void ratio. If e_0 was smaller than e_{max}, the shear curve had a measurable peak value and the conditioned sand exhibited strain-softening behavior. If e_0 was greater than e_{max}, the conditioned gravelly sand had a quite low strength. Different from fine-grained soils, the conditioned gravelly sands with e_0 smaller than e_{max} manifested an obvious stick-slip behavior.
- When e_0 was smaller than e_{max}, the initial void ratio decreased as the normal pressure increased, but the peak and residual strength increased. In addition, an increase in *FIR* significantly reduced the peak and residual strength. The residual strength and the corresponding void ratio of all specimens follow the same unique relation in the e-ln(τ) space. When e_0 was greater than e_{max}, the e_r-ln(τ_r) relation disobeyed the unique line. Note that the slump value offers a good correlation with the critical state strength under p=0.
- The conditioned gravelly sand with similar slump values but different water contents and *FIR*s showed various shear characteristics in pressurized conditions, indicating that the slump test hardly reflects the difference in conditioning state under $p > 0$.
- The coefficient of variation was proposed to assess the degree of stick-slip behavior in the residual stage caused by damage and reconnection of strong force chains between particles. The change in the coefficient of variation with normal pressure revealed that the stick-slip behavior of conditioned gravelly sands was more evident in a lower pressure state. However, the degree of the stick-slip behavior changed slightly with *FIR*.
- From a particle-scale perspective, it was revealed that the conditioning mechanism of foam was related to the weakening effect of foam bubbles on the stress-dependent interparticle friction. When e_r was smaller than e_{max}, the unique linear e_r-ln(τ_r) relation proved that foam bubbles could fill and expand the pores and then transfer the skeleton stress to pore pressure leading to less sliding friction. Furthermore, foam bubbles act as ball bearings and decrease the geometrical interlocking friction. When e_r was greater than e_{max}, the apparent cohesion produced by contractile skins contributed to the strength of foam-conditioned gravelly sand.

The results show that the shear characteristics and the conditioning mechanism of conditioned gravelly sands in pressurized chambers are different from those under $p = 0$, indicating the inadaptability of slump tests in characterizing the chamber muck fluidity and determining the optimal conditioning scheme. In addition, the measured residual strengths can characterize the muck fluidity in the numerical model of the muck movement in EPB shields. Moreover, the effect of shear rates and soil gradation characteristics on the shear strength of conditioned gravelly sands will be explored in the near future.

Acknowledgments

The financial support from the National Outstanding Youth Science Fund Project of the National Natural Science Foundation of China (No. 52022112), the National Natural Science Foundation of China (No. 52108388) and the Hunan Provincial Innovation Foundation for Postgraduate of China (No. 2020zzts152) are acknowledged and appreciated.

References

Adjemian, F. and Evesque, P. (2004), "Experimental study of stick-slip behavior", *Int. J. Numer. Anal. Method. Geomech.*, **28**(6), 501-530. https://doi.org/10.1002/nag.350.

Albert, I., Tegzes, P., Kahng, B., Albert, R., Sample, J.G., Pfeifer, M., Barabási, A.L., Vicsek, T. and Schiffer, P. (2000), "Jamming and fluctuations in granular drag", *Phys. Rev. Lett.*, **84**(22), 5122-5125.

ASTM D4648 (2011), *Standard test method for laboratory miniature vane shear test for saturated fine-grained clayey soil*, American Society for Testing and Materials, West Conshohocken, PA: ASTM, USA.

Bai, X.D., Cheng, W.C., Ong, D.E.L. and Li, G. (2021), "Evaluation of geological conditions and clogging of tunneling using machine learning", *Geomech. Eng.*, **25**(1), 59-73. https://doi.org/10.12989/gae.2021.25.1.059.

Bezuijen, A. (2012), "Foam used during EPB tunnelling in saturated sand, parameters determining foam consumption", *Proceedings of the World Tunnel Congress*, Bangkok, Thailand, January.

Budach, C. (2012), "Untersuchungen zum erweiterten Einsatz von Erddruckschilden in grobkörnigem Lockergestein", Ph.D. Dissertation, the Ruhr-Universität Bochum, Bochum, Germany.

Budach, C. and Thewes, M. (2015), "Application ranges of EPB shields in coarse ground based on laboratory research", *Tunn. Undergr. Sp. Tech.*, **50**, 296-304. https://doi.org/10.1016/j.tust.2015.08.006.

Cao, W.G., Wang, J.Y. and Zhai, Y.C. (2012), "Study of simulation method for the shear deformation of rock structural planes and interfaces with consideration of residual strength", *China Civil Eng. J.*. **45**(4), 127. (in Chinese)

Dang, T.S. and Meschke, G. (2020), "Influence of muck properties and chamber design on pressure distribution in EPB pressure chambers - Insights from computational flow simulations", *Tunn. Undergr. Sp. Tech.*, **99**, 103333. https://doi.org/10.1016/j.tust.2020.103333.

Duarte, M.Á.P. (2007), "Foam as a soil conditioner in tunnelling: physical and mechanical properties of conditioned sands", M.D. Dissertation, University of Oxford, UK.

EFNARC (2005), *Specifications and guidelines for the use of specialist products for mechanized tunnelling (TBM) in soft ground and hard rock*, European Federation of National Associations Representing for Specialist Construction Chemicals and Concrete systems, Farnham, UK.

Galli, M. and Thewes, M. (2019), "Rheological characterisation of foam-conditioned sands in EPB tunneling", *Int. J. Civ. Eng.*,

17(1), 145-160. https://doi.org/10.1007/s40999-018-0316-x.
GB/T50145 (2007), *Standard for engineering classification of soil,* Ministry of Water Resources of the People's Republic of China, Beijing, China. (in Chinese)
GB/T50123 (2019), *Standard for geotechnical test methods*, Ministry of Water Resources of the People's Republic of China, Beijing, China. (in Chinese)
Hu, W. and Rostami J. (2020), "A new method to quantify rheology of conditioned soil for application in EPB TBM tunneling", *Tunn. Undergr. Sp. Tech.*, **96**, 103192. https://doi.org/10.1016/j.tust.2019.103192.
Hu, W. and Rostami, J. (2021), "Evaluating rheology of conditioned soil using commercially available surfactants (foam) for simulation of material flow through EPB machine", *Tunn. Undergr. Sp. Tech*., **112**, 103881. https://doi.org/10.1016/j.tust.2021.103881.
Huang, S., Wang, S.Y., Xu, C.J., Shi, Y.F. and Ye, F. (2019), "Effect of grain gradation on the permeability characteristics of coarse-grained soil conditioned with foam for EPB shield tunnelling", *KSCE J. Civ. Eng.*, **23**(11), 4662. https://doi.org/10.1007/s12205-019-0717-7.
Jancsecz, S., Krause, R. and Langmaack, L. (1999), "Advantages of soil conditioning in shield tunnelling: experiences of LRTS Izmir", *Proceedings of the World Tunnel Congress on Challenges for the 21st Century.* Balkema, Rotterdam, Netherlands, May.
Liu, P.F., Wang, S.Y., Shi, Y.F., Yang, J.S., Fu, J.Y. and Yang, F. (2019), "Tangential adhesion strength between clay and steel for various soil softnesses", *J. Mater. Civ. Eng.*, **31**(5), 04019048. https://doi.org/10.1061/(ASCE)MT.1943-5533.0002680.
Liu, P.F., Wang, S.Y., Hu, Q.X. and Zhong, J.Z. (2020), "Effect of dispersant on the tangential adhesion strength between clay and metal for EPB shield tunnelling", *Tunn. Undergr. Sp. Tech.*, **95**, 103144. https://doi.org/10.1016/j.tust.2019.103144.
Martinelli, D., Peila, D. and Campa, E. (2015), "Feasibility study of tar sands conditioning for earth pressure balance tunnelling", *J. Rock Mech. Geotech. Eng.*, **7**(6), 684-690. https://doi.org/10.1016/j.jrmge.2015.09.002.
Martinelli, D., Winderholler, R. and Peila, D. (2017), "Undrained behaviour of granular soils conditioned for EPB tunnelling - A new experimental procedure", *Geomech. Tunn.*, **10**(1), 81-89. https://doi.org/10.1002/geot.201600019.
Martinelli, D., Todaro, C., Luciani, A. and Peila, D. (2019), "Use of a large triaxial cell for testing conditioned soil for EPBS tunnelling", *Tunn. Undergr. Sp. Tech.*, **94**, 103126. https://doi.org/10.1016/j.tust.2019.103126.
Meng, Q., Qu, F. and Li, S. (2011), "Experimental investigation on viscoplastic parameters of conditioned sands in earth pressure balance shield tunneling", *J. Mech. Sci. Technol.*, **25**(9), 2259-2266. https://doi.org/10.1007/s12206-011-0611-9.
Mori, L., Mooney, M. and Cha, M. (2018), "Characterizing the influence of stress on foam conditioned sand for EPB tunneling", *Tunn. Undergr. Sp. Tech.*, **71**, 454-465. https://doi.org/10.1016/j.tust.2017.09.018.
Peila, D., Oggeri, C. and Borio, L. (2009), "Using the slump test to assess the behavior of conditioned soil for EPB tunneling", *Environ. Eng. Geosci.*, **15**(3), 167-174. https://doi.org/10.2113/gseegeosci.15.3.167.
Peila, D. (2014), "Soil conditioning for EPB shield tunneling", *KSCE J. Civ. Eng.*, **18**(3), 831-836. https://doi.org/10.1007/s12205-014-0023-3.
Qu, T.M., Feng, Y.T., Wang, Y. and Wang, M. (2019), "Discrete element modelling of flexible membrane boundaries for triaxial tests", *Comput. Geotech.*, **115**, 103154. https://doi.org/10.1016/j.compgeo.2019.103154.
Qu, T.M., Di, S.C., Feng, Y.T., Wang, M. and Zhao, T.T. (2021), "Towards data-driven constitutive modelling for granular materials via micromechanics-informed deep learning", *Int. J. Plast.*, **144**, 103046. https://doi.org/10.1016/j.ijplas.2021.103046.
Quebaud, S., Sibai, M. and Henry, J.P. (1998), "Use of chemical foam for improvements in drilling by earth-pressure balanced shields in granular soils". *Tunn. Undergr. Sp. Tech.*, **13**(2), 173-180. https://doi.org/10.1016/S0886-7798(98)00045-5.
Terzaghi, K., Peck, B.R. and Mesri, G. (1996), *Soil Mechanics in Engineering Practice (3rd Ed.)*, John Wiley & Sons, Inc, New York, NY, USA.
Thewes, M. and Hollmann, F. (2016), "Assessment of clay soils and clay-rich rock for clogging of TBMs", *Tunn. Undergr. Sp. Technol.*, **57**, 122-128. https://doi.org/10.1016/j.tust.2016.01.010.
Vinai, R., Oggeri, C. and Peila, D. (2008), "Soil conditioning of sand for EPB applications: A laboratory research". *Tunn. Undergr. Sp. Technol.*, **23**(3), 308-317. https://doi.org/10.1016/j.tust.2007.04.010.
Wang, S.Y., Hu, Q.X., Wang, H.B., Thewes, M., Ge, L., Yang, J.S. and Liu, P.F. (2020), "Permeability characteristics of poorly graded sand conditioned with foam in different conditioning states", *J. Test. Eval.*, **49**(5), 3620-3636.
Wang, H.B., Wang, S.Y., Zhong, J.Z., Qu, T.M., Liu, Z.R., Xu, T. and Liu, P.F. (2021), "Undrained compressibility characteristics and pore pressure calculation model of foam-conditioned sand", *Tunn. Undergr. Sp. Tech.*, **118**, 104161. https://doi.org/10.1016/j.tust.2021.104161.
Xu, J.S. and Du, X.L. (2019), "Energy analysis of geosynthetic-reinforced slope in unsaturated soils subjected to steady flow", *J. Cent. South Univ.*, **26**, 1769-1779. https://doi.org/10.1007/s11771-019-4132-5.
Yang, Y., Li, X.G. and Su, W.L. (2020), "Experimental investigation on rheological behaviours of bentonite- and CMC-conditioned sands", *KSCE J. Civ. Eng.*, **24**(6), 1914-1923. https://doi.org/10.1007/s12205-020-2035-5.
Ye, X.Y., Wang, S.Y., Yang, J.S., Sheng, D.C. and Xiao, C. (2016), "Soil conditioning for EPB shield tunneling in argillaceous siltstone with high content of clay minerals: Case study", *Int. J. Geomech.*, **17**(4), 05016002.
Zhang, L. (2014), "Study on rheological properties of conditioned sandy pebble soil based on DEM", PhD Dissertation, China University of Geosciences (Beijing), Beijing, China. (in Chinese)
Zhang, X.D. (2009), "Construction technology of earth pressure balance shield in watery sandy stratum", *Chinese J. Geotech. Eng*., **31**(9), 1445-1449. (in Chinese)
Zhao, B.Y., Liu, D.Y. and Jiang, B. (2018), "Soil conditioning of waterless sand–pebble stratum in EPB tunnel construction", *Geotech. Geol. Eng.*, **36**, 2495-2504.
Zhong, J.Z., Wang, S.Y., Liu, P.F. and Wang, H.B. (2021), "Mechanical behavior and rheology model of foam-conditioned gravelly sand in EPB shield tunneling", *J. Harbin Inst. Technol.*, **53**(11), 84-92. (in Chinese)
Zhong, J.Z., Wang, S.Y., Liu, P.F., Liu, Z.R. and Xu, T. (2022), "Investigation of the dynamic characteristics of Muck during EPB shield tunnelling in a full chamber model using a CFD method", *KSCE J. Civ. Eng.*, **26**(9), 4103-4116. https://doi.org/10.1007/s12205-022-1300-1.
Zumsteg, R., Plötze, M. and Puzrin, A.M. (2012), "Effect of soil conditioners on the pressure and rate-dependent shear strength of different clays". *J. Geotech. Geoenviron. Eng.*, **138**(9), 1138-1146. https://doi.org/10.1061/(ASCE)GT.1943-5606.00006.

IC